Enhancing Beat-to-Beat Analysis of Heart Signals With Respiration Harmonics Reduction Through Demodulation and Template Matching

Jannatun Noor Sameera[®], *Graduate Student Member, IEEE*,
Mohammad Shadman Ishrak, *Graduate Student Member, IEEE*, Victor M. Lubecke[®], *Fellow, IEEE*,
and Olga Boric-Lubecke, *Fellow, IEEE*

Abstract—Heart rate variability (HRV) analysis using Doppler radar (DR) is a promising method for noninvasive health and stress assessment. However, the respiration signal harmonic content typically limits HRV parameter estimation accuracy. While several harmonic reduction techniques have been used to improve the average HR estimation accuracy, achieving high beat-to-beat interval (BBI) accuracy is still challenging. This article demonstrates that arctangent demodulation (AD) with wavelet-based signal processing enhanced with template matching is effective to estimate HRV parameters with accuracy on the order of 10 ms with 2.4 GHz DR. Moreover, it was theoretically and experimentally demonstrated that the cases where AD provides limited improvement due to phase delay between thorax and abdomen motion are easily identifiable, and can be alternatively processed using a single-channel data.

Index Terms—Doppler radar (DR), heart rate monitoring, heart rate variability (HRV) analysis, multiresolution analysis, noncontact monitoring, respiration harmonics, template matching filtering.

I. INTRODUCTION

THE use of Doppler radar (DR) for physiological sensing was first demonstrated in the 1970s [1], [2]. Since then vital signs monitoring using DR sensors is becoming increasingly popular due to its unobtrusive and noncontact nature [3], [4]. Besides finding heart rate and respiration rate, DR can be employed for more sophisticated analysis such as heart rate variability (HRV). In contrast to traditional methods such as electrocardiogram (ECG), photoplethysmography (PPG), spirometry, etc., radar sensors can be employed for such analysis without requiring any physical connection to the patient's body.

Manuscript received 11 July 2023; revised 8 September 2023; accepted 26 September 2023. Date of publication 26 October 2023; date of current version 10 January 2024. This work was supported by the National Science Foundation (NSF) under Grant IIS1915738 and Grant CNS2039089. (Corresponding author: Januarun Noor Sameera.)

This work involved human subjects or animals in its research. Approval of all ethical and experimental procedures and protocols was granted by the University of Hawaii Human Studies Program's Institutional Review Board (IRB) under Application No. CHS 14884. "Remote Sensing of Physiological Motion Using Doppler Radar" protocol.

The authors are with the Electrical and Computer Engineering Department, University of Hawaii at Manoa, Honolulu, HI 96822 USA (e-mail: jsameera@hawaii.edu; ishrak@hawaii.edu; lubecke@hawaii.edu; olgabl@hawaii.edu).

Color versions of one or more figures in this article are available at https://doi.org/10.1109/TMTT.2023.3324444.

Digital Object Identifier 10.1109/TMTT.2023.3324444

HRV refers to the time alterations in the beat-to-beat interval (BBI) of heart signals and can index autonomic nervous system (ANS) activity. Hence, it reflects how the cardiovascular regulatory system responds to demand, stress, and illness. Reduced HRV has been associated with decreased vagal activity [5]. Furthermore, HRV can be used to predict the prognosis of cardiovascular diseases and the onset of metabolic disorders. In a recent work by Ahmed et al. [6], an IR-UWB radar was employed to measure HRV during rest and fatigued states. Another study presented a fast and real-time HRV extraction using a compact 24-GHz continuous wave (CW) DR. The study introduced a computationally intensive algorithm using bandpass filter banks to determine the heart signal [7]. In another study, an algorithm for detecting peaks of the heart signal was introduced for HRV analysis to predict drowsiness [8]. However, peak detection of heart signals is severely affected by the presence of respiration harmonics in the DR output. Respiratory signals have amplitudes ranging from 4 to 12 mm and a normal respiratory rate of 5-25 breaths per minute (b/m). In contrast, heartbeat signals have amplitudes ranging from 0.2 to 0.5 mm and a normal heart rate of 50–120 beats per minute (bpm) [7]. The significant difference in amplitude between respiratory and heartbeat signals makes respiratory harmonics a source of interference in identifying heartbeat signals. When the harmonics are close in frequency or have similar amplitudes to the heart fundamental, it can result in incorrect peak detection and consequently lead to inaccurate HRV analysis [9], [10].

A study [11] presented the use of an adaptive harmonic comb notch filter, which consists of multiple notches at respiration frequencies and harmonics, with a magnitude determined by the ratio of harmonic amplitude. In order to combat such harmonic interference, Tu and Lin [12] proposed the use of complex signal demodulation that does not require compensation of dc offset which is another challenge in DR signals [3]. Another study involves the Hough transform that accumulates signal energy along a preset frequency trajectory for extracting heartbeat signals [13]. Alternatively, higher order respiration harmonics have also been used for separating heart and respiration signals using an adaptive harmonic cancellation filter method based on the least mean square algorithm [14]. However, these studies were limited to only separating heart signals and accurate extraction of

0018-9480 © 2023 IEEE. Personal use is permitted, but republication/redistribution requires IEEE permission. See https://www.ieee.org/publications/rights/index.html for more information.

average heart rate. Studies concerning instantaneous heart rate measurement, HRV analysis, etc. became very inaccurate in the presence of such harmonics. Correct BBI estimation is a foundation for accurate HRV analysis.

This article builds upon our previous study [9], which introduced a method using the maximal overlap discrete wavelet transform (MODWT) to reduce harmonic interference in beat-to-beat analysis for single channel and linearly demodulated signals. The average error in average heart rate extraction varied from 0.47 to 3.64 bpm. The difference between the standard deviation of NN intervals (SDNN) extracted from radar and PPG signal was reported to be 71 ms on average.

This article focuses on mitigating respiration harmonics by employing arctangent demodulation (AD) and presenting an algorithm for reducing such interferences in heart signals. This algorithm applies multiresolution analysis MODWT to the filtered signals after AD, followed by the utilization of a template matching filter (TMF) and peak detection method to identify accurate peaks in the heart signals [15]. These processing steps have resulted in significant and consistent improvement in BBI estimation, resulting in highly accurate HRV parameters: SDNN accuracy of 10.71 ms, and RMSDD accuracy of 14.16 ms. These results present the highest HRV accuracy reported to date with a 2.4-GHz radar system with a low sampling rate of 100 Hz.

This article is organized as follows. Section II provides theoretical analysis and simulation results assessing the sensitivity of respiration harmonics to breathing features and demodulation methods. Section III describes the data collection protocol, while Section IV quantifies the reduction of harmonics achieved through the use of AD and provides an explanation for the varying degree of reduction among subjects. Section V introduces a proposed algorithm for beat-to-beat analysis of heart signals, evaluates the accuracy of the proposed algorithm in terms of HRV features, and compares it with existing methods. Finally, Section VI concludes the article with a discussion and outlines future plans.

II. DR SYSTEM

The fundamental principle of using DR for physiological motion sensing is to analyze the time-varying phase shift in the received signal caused by chest wall movement due to heart and respiratory efforts. Fig. 1 shows the block diagram of the CW quadrature channel DR operating at 2.4 GHz. To avoid the demodulation sensitivity to the target's position, a quadrature receiver is chosen instead of a single-channel radar system [16].

The RF wave reflected at the chest wall undergoes nonlinear phase modulation which can be denoted by θ which is dependent on the nominal distance between the target and the antenna. The received I and Q baseband outputs can be expressed as

$$B_I(t) = A_B \cos \left(\theta + \frac{4\pi x(t)}{\lambda} + \Delta \phi(t)\right) \tag{1}$$

$$B_{Q}(t) = A_{B} \sin \left(\theta + \frac{4\pi x(t)}{\lambda} + \Delta \phi(t)\right)$$
 (2)

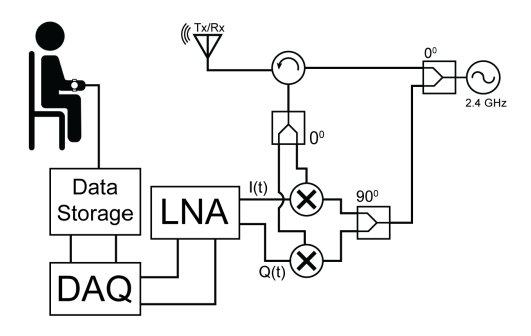


Fig. 1. Block diagram of a quadrature CW DR [9].

where the baseband amplitude due to receiver and mixer gain is given by A_B , the target's time-varying displacement is given by x(t), and the residual phase noise is given by $\Delta \phi(t)$ [16]. Considering the equation for the I-channel baseband output, it can be approximated and represented in its equivalent Fourier series as follows:

$$B_{I}(t) \approx \cos\left[\frac{4\pi x(t)}{\lambda} + \Phi\right]$$

$$= \sum_{n=-\infty}^{\infty} J_{n}\left(\frac{4\pi m}{\lambda}\right) \cos(n\omega + \Phi)$$
 (3)

where, ϕ represents the total phase shift (i.e., $\Delta \phi(t) + \theta$) and J_n denotes the Bessel function of the first kind. Different values of n correspond to different frequency components of $B_I(t)$. Hence, this nonlinear property of the cosine transfer function results in harmonic interference in the baseband spectrum [10]. The harmonic content depends on the total phase shift ϕ , which is a function of the distance between the radar antenna and the target, and the features of the chest wall motion x(t), which includes breathing and heart motion.

A simulation is performed to illustrate how harmonic content varies with the total phase shift using MATLAB. A sinusoidal half cycle with a rounded cusp can be taken as an idealized chest motion due to respiration [17]

$$p_R(t) = \sin^p \pi f_R(t) \tag{4}$$

where f_R is the respiratory frequency and p manipulates the rounding of the cusp. The heart motion can be modeled with an analog pulse of an exponential $e^{\frac{t}{\tau}}$ having a time constant of τ with a critically damped second-order Butterworth filter

$$p_H t = e^{\frac{-t}{\tau}} + \left[\left(\frac{\sqrt{2}}{\omega_o \tau} - 1 \right) \sin \frac{\omega_o t}{\sqrt{2}} - \cos \frac{\omega_o t}{\sqrt{2}} \right] e^{-\frac{\omega_o \tau}{\sqrt{2}}}. \quad (5)$$

 f_o represents the cut-off frequency of the filter and f_H denotes the heartbeat frequency [17]. The orthonormal baseband outputs are simulated with x(t) as a combination of $p_R(t)$ and $p_H(t)$. Assuming the initial angle to be θ_o , the constant phase shift can be written as

$$\theta = \frac{4\pi}{\lambda} D - \theta_{\circ}. \tag{6}$$

Here, D is the nominal distance between the target and the antenna. The initial angle is taken to be equivalent to phase change at the reflection surface.

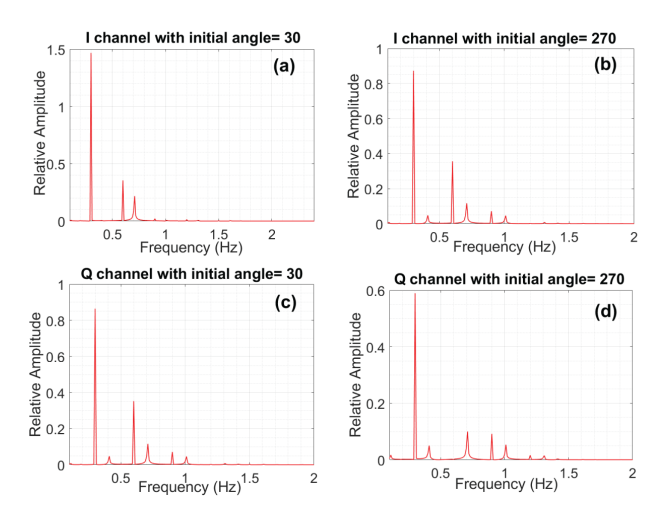


Fig. 2. FFT of simulated I and Q channel signals at different phase shifts, illustrating the corresponding variation in harmonic content. (a) I channel with initial angle = 30. (b) I channel with initial angle = 270. (c) Q channel with initial angle = 270.

To illustrate the origin of harmonics due to the cosine transfer function in the baseband output, the FFT plot of simulated I and Q channel signals at different phase shifts is shown in Fig. 2. It can be seen that the harmonic contents vary as the phase shift is varied.

To overcome the issue associated with cosine transfer function dependency, AD can be applied to the ratio of the two orthonormal outputs to obtain phase information directly.

The amplitude and phase imbalance between the two channels must be compensated before demodulation to avoid magnifying the harmonics [18]. The dc offset is compensated using a circle-fitting method based on the Levenberg–Marquardt (LM) algorithm. The phase shift caused by the chest wall displacement due to cardiopulmonary activity can be extracted from such a nonlinear demodulation technique, which is written as

$$\theta_{AD}(t) = \arctan \frac{B_{\mathcal{Q}}(t)}{B_{I}(t)}$$

$$= \arctan \left(\frac{\sin \left(\frac{4\pi x(t)}{\lambda} + \Delta \Phi(t) + \theta \right)}{\cos \left(\frac{4\pi x(t)}{\lambda} + \Delta \Phi(t) + \theta \right)} \right)$$

$$= \frac{4\pi x(t)}{\lambda} + \Delta \Phi(t) + \theta. \tag{7}$$

Since the demodulated output does not contain the cosine transfer function, the harmonic interference can be attenuated with AD.

However, respiration harmonics are also inherent to breathing features. The respiration model used in (4) is an example of a typical breathing motion that includes higher harmonics. In addition, time delay between thoracic and abdominal motion also produces respiration harmonics. During inhalation, air fills the thorax first, then the abdomen expands. Similarly, the exhalation process starts earlier for the thorax. Since the abdomen motion is delayed with respect to the thorax, the overall torso moves in a short nonuniform ripple, which directly affects the effective radar cross section. Hence, the characteristics of respiratory motion vary between humans [19].

To illustrate this, a simulation study is carried out where the reflected wave from the moving torso is represented as the superposition of two components that are different in amplitude with a phase offset. For this simulation, the baseband outputs are modified where the heart motion is neglected for simplicity

$$B_{I}(t) = A_{T} \cos \left[\frac{4\pi}{\lambda} x_{R}(t) + \phi_{\text{tot}} \right]$$

$$+ A_{A} \cos \left[\frac{4\pi}{\lambda} [x_{R}(t - t_{d})] + \Phi_{\text{tot}} + \alpha \right]$$

$$B_{Q}(t) = A_{T} \sin \left[\frac{4\pi}{\lambda} x_{R}(t) + \phi_{\text{tot}} \right]$$

$$+ A_{A} \sin \left[\frac{4\pi}{\lambda} [x_{R}(t - t_{d})] + \Phi_{\text{tot}} + \alpha \right]$$

$$(9)$$

where, the amplitudes of the components from the thorax and abdomen are given by A_T and A_A , respectively, α is the phase offset due to the difference in the nominal target range, t_d is the time delay of the abdomen motion and the roundtrip phase offset is given by ϕ_{tot} . These two equations are further simplified by taking a respiration rate of 18 b/m and setting $u = \frac{A_A}{A_T}$ with $A_T = 1$. Since a 2.4-GHz radar is used in this study, the wavelength is set to 12.5 cm for this simulation

$$B_{I}(t) = \cos[\cos(2\pi \cdot 0.3 \cdot t)]$$

$$+ u \cdot \cos\left[\cos(2\pi \cdot 0.3 \cdot t) + \frac{\pi}{k} + \frac{\pi}{n}\right] \qquad (10)$$

$$B_{Q}(t) = \sin[\cos(2\pi \cdot 0.3 \cdot t)]$$

$$+ u \cdot \sin\left[\cos(2\pi \cdot 0.3 \cdot t) + \frac{\pi}{k} + \frac{\pi}{n}\right]. \qquad (11)$$

The phase offsets caused by the abdomen motion delay and the difference in levels are expressed with the variables k and n, respectively [19]. The IQ plot and frequency domain plots of the single channel and AD signals are presented for three cases. The first case is when the phase shift and motion delay is at 30° and 23° , respectively.

To illustrate the worst case scenario, n is set to 2 and 8, respectively. Fig. 3 illustrates these cases and it can be seen that with increasing phase shift and motion delay, the harmonic contents in the single-channel signals also increase. Hence, when the phase shift is increased to 90°, the harmonics attenuation with arctangent demodulated signal decreases as well. With increasing phase offset, AD loses its merits. Fig. 3(g)–(i) illustrates that the demodulation becomes inaccurate due to the incorrect circle-fitting method in the worst case scenario with 180° phase offset referring to the case where the thorax and abdomen move in completely opposite directions. As a result, the harmonics reduction is also severely affected.

III. DATA COLLECTION PROTOCOL

For this study, data is collected from four subjects breathing at a fixed breathing rate of 13, 15, and 18 b/m with the aid of a metronome. As shown in Fig. 1, an E4433B signal generator is used as a signal source at 2.4 GHz and amplitude of 16 dBm. Additionally, the radar setup included ZFM4212 mixers, ZX10Q-2-25S+ 90° splitter, and a Narda 4923. Mixers' outputs are low pass filtered at 10 Hz and passed through

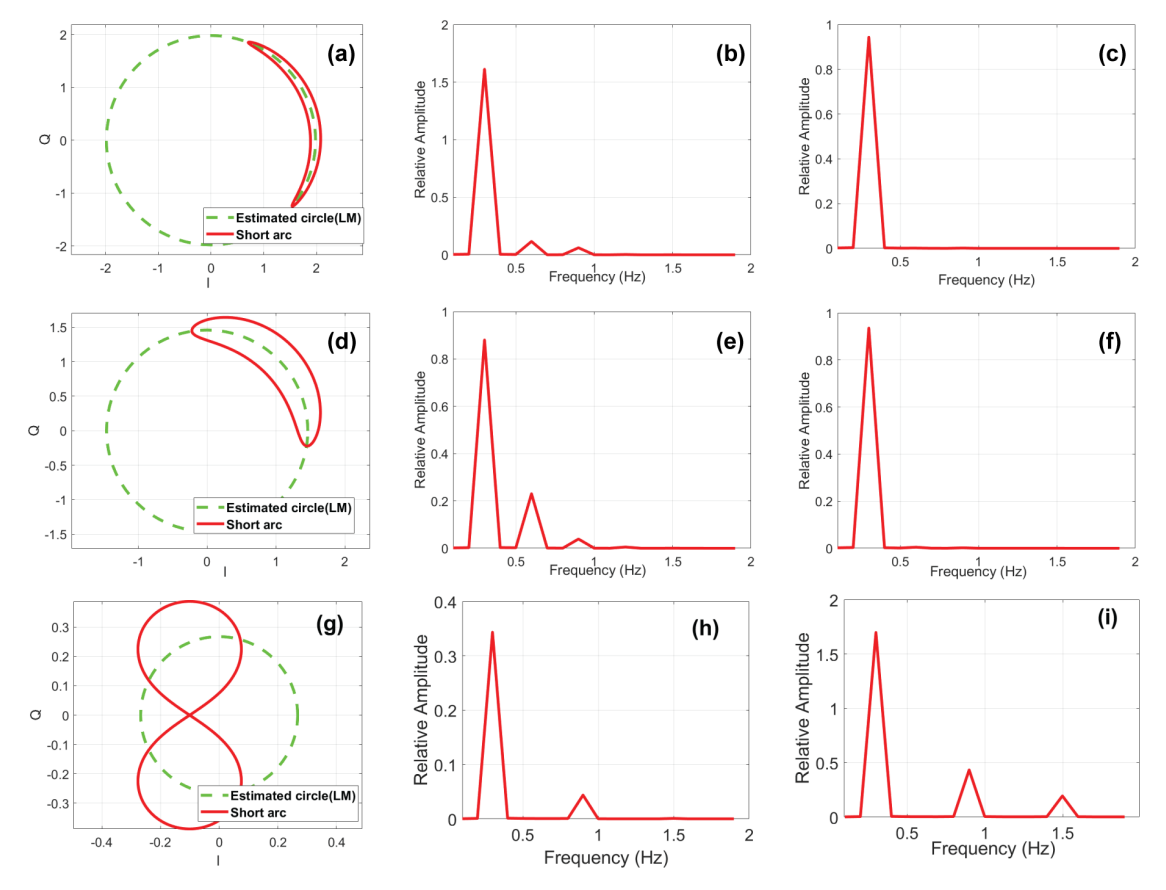


Fig. 3. Simulated graphs showing (a) IQ plot, (b) FFT plot of single-channel signal, and (c) FFT plot of AD signal when phase delay = 30° and motion delay = 23° . (d)–(f) Corresponding graphs of phase delay increased to 90° . LM algorithm fails at phase offset = 180° in (g) causing incorrect AD and higher harmonics in (h) and (i).

a dc-coupled SR560 LNA for amplification of the signals. Finally, the I and Q outputs are recorded with an 18-bit DAQ at a sampling rate of 100 Hz. PPG signal is collected as a reference signal from the right-hand wrist of the subject. For this purpose, a wrist-based watch containing SpO2, HR, and HRV health sensor platform, MAXREFDES103 is employed. The watch operates in transmission mode by utilizing a green LED light to measure the volumetric variations of blood circulation. PPG data from this watch is recorded at a 100-Hz sampling rate using the Maxim Integrated software. Data from the radar and watch is aligned using the timestamps. To derive the imbalance factors, data from a mechanical mover with a spherical surface moving at a fixed frequency with a 4-cm peak-to-peak amplitude is taken [20]. The amplitude and phase imbalance factors are calculated using the algebraic ellipse fitting method. These values are used to correct the imbalance in human data using the Gram-Schmidt method before demodulating the single-channel signals [20], [21].

IV. RESPIRATION HARMONICS CANCELLATION

In this section, the effect of AD in harmonics reduction is presented. To better assess the harmonic contents, the signals are filtered from 0.05 to 1 Hz with a bandpass filter of 600th order. The power spectrum for the two single-channel signals and the arctangent demodulated signal is plotted in Fig. 4. In contrast to the single-channel signals, the power of

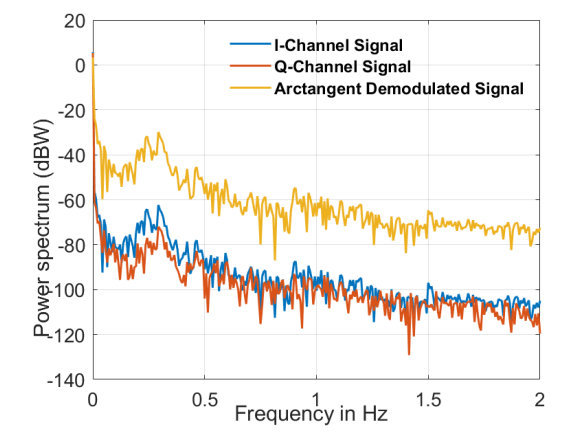


Fig. 4. Power spectrum of the single-channel signals along with the arctangent demodulated signal.

fundamental respiratory frequency is much higher compared to that of the harmonics in the demodulated signal. This is further illustrated in Fig. 5, which shows the percentage of the amplitude of the second (H2) and third (H3) harmonics with respect to the amplitude of fundamental frequency for each of these signals.

As can be seen from Fig. 5, the percentage amplitude (PA) of harmonics for Subject A reduces when the single-channel

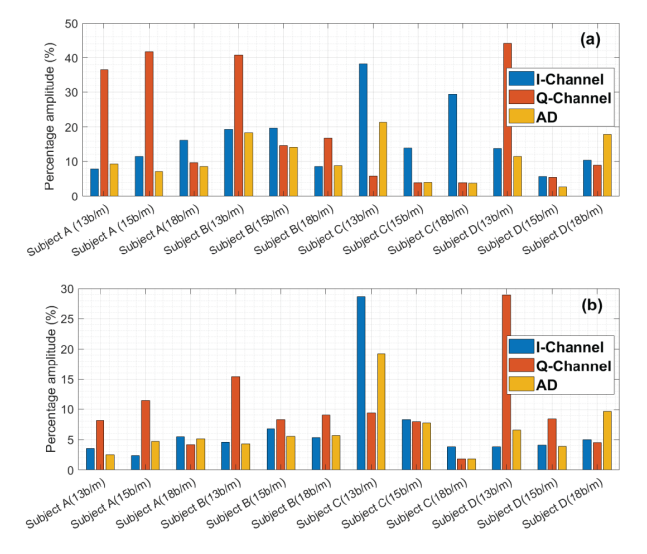


Fig. 5. Percentage of the amplitude of (a) second and (b) third harmonics, relative to the amplitude of the fundamental respiration frequency.

signals are demodulated for all three breathing rates. For the dataset from Subject A at 13 b/m, the PA decreased from 36.57% with the Q-channel signal to 9.32% with AD. In this case, the highest harmonic reduction using demodulated signal is 83.03% with respect to the Q-channel signal with a breathing rate of 15 b/m. However, for Subject B, the decrease in PA is not as significant compared to the former subject. For example, with Subject B at 15 b/m, the PA decreases from 19.73% to 14.04% when the demodulated signal is used instead of the I-channel signal. For Subject-C, this reduction deteriorated further where the demodulated signal shows a lower decrease in PA than the Q-channel signal when the breathing rate is at 13 and 15 b/m. This can be attributed to the increased phase offset between the abdomen and thorax as explained in Section II.

Fig. 6 illustrates the *IQ* plot of approximately one breathing cycle of Subject A and Subject C with both at 13 b/m. It can be seen that the *IQ* plot of Subject C is hollower compared to Subject A, which indicates the higher phase offset in the torso in the former subject [20]. As shown in Fig. 3, with increasing phase offset, AD becomes less accurate, and hence resulting harmonic attenuation is also decreased.

Lastly, for Subject D, the harmonic distortion can be seen to be reduced in Fig. 5 in the demodulated signal compared to single-channel signals. The PA of second harmonics in the 15 b/m dataset of this subject is 5.52% and it decreases by 52% with demodulation. However, when the subject's breathing rate is increased to 18 b/m, the harmonic distortion becomes higher in the demodulated signal compared to the single-channel signals.

V. BEAT-TO-BEAT ANALYSIS

A. Proposed Algorithm

The algorithm employed for processing the radar signal for beat-to-beat analysis of the heart signal is shown in Fig. 7. The arctangent demodulated output is at first unwrapped and then filtered with a bandpass FIR filter to attenuate the respiratory

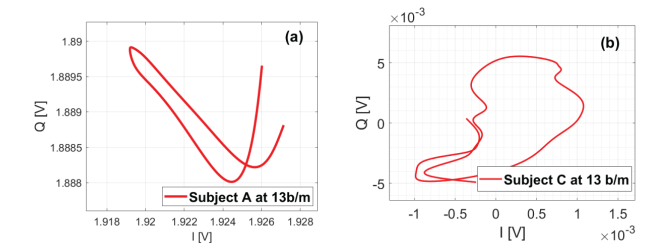


Fig. 6. IQ plot of approximately one breath. (a) Subject A at 13 b/m and (b) subject C at 13 b/m.

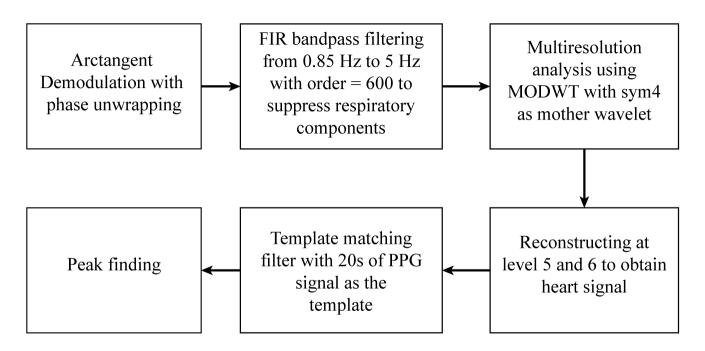


Fig. 7. Digital signal processing algorithm prior to peak detection in heart signals.

signal. Next, the signal is passed through the multiresolution analysis MODWT. It uses Symlet (sym) four mother wavelet to decompose the filtered AD signal into 12 different levels where smaller levels refer to the higher frequencies. It does so by transforming the input signal into detail coefficients and scaling coefficients with respect to variations over a set of scales.

The convolution of MODWT for a time series $C_{(o,n)}^{(M)} = x_n$ can be written as

$$d_{j,n}^{(M)} = \sum_{l=0}^{L-1} \tilde{h}_L C_{j-1}^{(M)}, (n-2^{j-1}l) \mod N$$
 (12)

$$C_{j,n}^{(M)} = \sum_{l=0}^{L-1} \tilde{g}_L C_{j-1}^{(M)}, (n-2^{j-1}l) \mod N$$
 (13)

where, $d_{j,n}^{(M)}$ and $C_{j,n}^{(M)}$ are the wavelet and scaling coefficients, respectively, $n = 0, 1, \ldots, N-1$ denotes the length of time series. M stands for MODWT.

Unlike discrete wavelet transform, MODWT suffers less from boundary effects as its decomposed level is defined for any sample size. Furthermore, MODWT offers better alignment of decomposed wavelet and scaling coefficients at each level with the original time series. As a result, the analysis of localized signal variation with respect to scale and time is easier with this process [22]. Next, the reconstructed signal at levels 5 and 6 is passed through the TMF. This adaptive approach emphasizes the input signal by convolving it with another signal used as a template. This is an optimal filter and the maximum signal-to-noise ratio of the output signal is its optimal criterion [23].

The effectiveness of a TMF lies in the proper selection of the template signal. In some studies, a polynomial approximation is utilized to create a template in a 2-s time window [24].

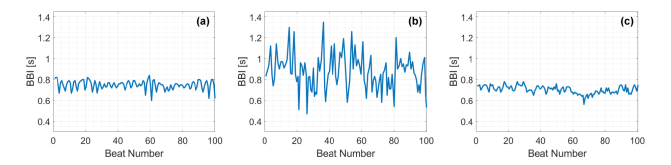


Fig. 8. Tachogram of the BBI from demodulated signals (a) with the proposed algorithm, (b) without the proposed algorithm, and (c) PPG signal of Subject D at 15 b/m.

Methods such as singular value decomposition [22] and eigenvector-based spatial filtering [25] are also proposed to generate the templates. Furthermore, the heart signal captured keeping breath held for a few seconds has been used as a template signal for studying HRV [15]. In this experiment, the template is generated by filtering a 20-s segment of the reference PPG signal. Next, according to the TMF algorithm, the time-reversed and conjugated version of the template signal is convolved with the reconstructed signal.

Assuming x[n] to be the reconstructed signal and h[n] as the template signal, the TMF operation can be given as

$$x_h[n] = x[n] * h^*[-n]$$
 (14)

where $x_h[n]$ is the output signal. Finally, the peaks of the output signal as well as the reference PPG signals are identified [26]. The BBIs obtained with and without the algorithm are shown in Fig. 8, along with the reference PPG signal. The proposed algorithm effectively reduces harmonics in the demodulated radar signal, resulting in a significant decrease in false peaks. The AD signal with the algorithm exhibits missing peaks and noise interference, which are more frequent in the AD signal without the algorithm. Furthermore, the BBI variability in the signal in Fig. 8(b) does not match the reference signal and numerous false peaks are detected, mainly due to harmonics interference, which is significantly reduced when the algorithm is applied.

The average heart rate of the subjects at different breathing rates is determined and listed in Table I. The proposed algorithm presents a computationally effective and fast method to extract heart rate using simple radar architecture. The mean of the difference between average heart rates extracted from the radar and the PPG is 1.56 BPM with a standard deviation of 1.41 BPM with a mean absolute error (MAE) of 19 ms for the extracted BBIs. This accuracy is within the expected resolution for a low sampling rate of 100 Hz.

Furthermore, the Bland–Altman plots are presented in Fig. 9 to assess the accuracy of the algorithm in determining correct BBIs from the radar signal. The bias in such plots refers to the average of all differences between the BBIs extracted from the radar signals and the reference PPG signal. The limits of agreement between the BBIs of these two signals are defined by the 95% confidence interval. The analysis shows satisfactory agreement between the BBIs from two signals at varying breathing rates, which shows the reliability of the proposed method in removing the harmonics to improve the beat-to-beat analysis of heart signals.

TABLE I Average Heart Rate Extracted Using the Proposed Algorithm for All Datasets

Dataset	Average heart rate (BPM)			
Datasct	Radar	PPG		
Subject A (13b/m)	67.63	69.29		
Subject A (15b/m)	66.59	65.48		
Subject A (18b/m)	69.86	67.32		
Subject B (13b/m)	65.58	62.97		
Subject B (15b/m)	59.87	60.09		
Subject B (18b/m)	59.32	60.52		
Subject C (13b/m)	65.23	63.99		
Subject C (15b/m)	64.88	65.20		
Subject C (18b/m)	68.70	68.03		
Subject D (13b/m)	79.31	79.33		
Subject D (15b/m)	80.34	85.44		
Subject D (18b/m)	81.88	84.02		

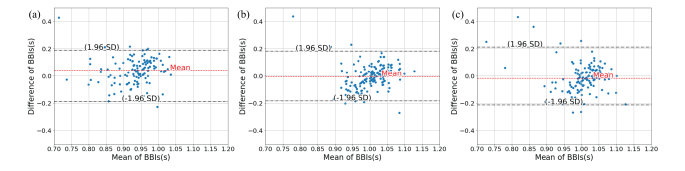


Fig. 9. Bland–Altman plots for BBI measurements for datasets from Subject B at (a) 13, (b) 15, and (c) 18 b/m, respectively.

B. HRV Features

For this analysis, the HRV features extracted from the beat-to-beat analysis are the standard deviation of BBIs (SDNN) and the root mean square of successive differences (RMSSD). Since all the datasets in this study were at most 2 min long, these two features are used for their suitability in short-term measurement [27]. SDNN is a measure of overall ANS activity. RMSSD is a measure of high-frequency HRV, and it reflects the integrity of the vagus nerve-meditated autonomic control of the heart [27].

If a heartbeat N occurs at time t(n) where $n \in 1, N$, the interval between the beats can be denoted by $\delta(n) = t(n) - t(n-1)$, and the average BBI can be denoted by $\bar{\delta}$. Hence, SDNN and RMSSD can be measured using the following two equations:

SDNN =
$$\sqrt{\frac{1}{N-2} \sum_{n=2}^{N} (\delta(n) - \bar{\delta})^2}$$
 (15)

RMSSD =
$$\sqrt{\frac{1}{N-2} \sum_{n=3}^{N} [\delta(n) - \delta(n-1)]^2}.$$
 (16)

These two features extracted from the PPG and the heart signal after applying the proposed algorithm are summarized in Table II.

To better assess the improvement in beat-to-beat analysis resulting from the harmonic attenuation by using AD, these features are also obtained with a single-channel signal with a lower harmonic content (Fig. 5). In all cases, AD accuracy is within 38 ms with an average accuracy of 12.43 ms, whereas single-channel accuracy is within 55 ms. This accuracy is within the resolution for a 100-Hz sampling rate. Overall AD accuracy is significantly higher than single-channel accuracy,

Dataset	SDNN (ms)			RMSSD (ms)			
Dataset		Radar			Radar		
	Radar	(Single	PPG	Radar	(Single	PPG	
	(AD signal)	Channel		(AD signal) Channe		110	
		signal)			signal)		
Subject A (13b/m)	64.83	107.13	68.55	58.36	116.84	74.26	
Subject A (15b/m)	58.03	71.74	32.89	40.66	84.56	31.52	
Subject A (18b/m)	42.09	61.34	34.89	43.09	49.74	27.96	
Subject B (13b/m)	72.11	66.77	76.99	68.00	58.58	72.79	
Subject B (15b/m)	75.70	54.58	71.79	83.54	59.67	78.19	
Subject B (18b/m)	82.05	90.75	76.32	77.31	73.28	72.52	
Subject C (13b/m)	28.83	36.23	41.63	28.04	31.78	37.62	
Subject C (15b/m)	44.87	51.81	32.18	29.52	53.59	25.62	
Subject C (18b/m)	19.16	24.69	31.15	15.75	24.86	34.12	
Subject D (13b/m)	54.01	68.75	40.08	56.17	87.29	32.70	
Subject D (15b/m)	42.57	54.41	37.02	51.91	62.45	29.37	
Subject D (18b/m)	56.21	46.86	35.22	65.05	51.83	28.02	

TABLE II
EXTRACTED HRV FEATURES FROM BEAT-TO-BEAT ANALYSIS FOR ALL DATASETS

TABLE III

COMPARING THE ACCURACY OF HRV FEATURES BETWEEN THE PUBLISHED DATA AND THE PROPOSED METHOD

	Radar System	Sampling rate (Hz)	Data collection setup	Mean Average Error (ms)		Method	
	Samping rate (nz) Data conection setup		SDNN	RMSSD			
[5]	CW Quadrature Radar at	1000	Seated position	20.15	194.84	Robust autocorrelation on linearly	
[2]	2.4 GHz operating frequency	1000	Scated position	20.13		demodulated signals	
[7]	CW Quadrature Radar at	1000	Seated position	1.97	2.86	Narrowband band pass filter bank	
[[/]	24 GHz operating frequency	1000	•	12.25	20.75	Chirp Z-transform	
[8]	CW Quadrature Radar at	1000	Supine position in wake state	120.25	242.36	Peak detection alogirthm based on windows.	
[6]	2.45 GHz operating frequency	1000	Supine position in drowsy state	171.39	348.95		
[28]	CW Quadrature Radar at	50000 Seated position		2.56	6.37	Decoding peak detection	
[20]	24 GHz operating frequency	30000	Scatca position	2.36	7.05	Hidden semi-Markov model-based	
				2.30 7.03		radar signal segmentation	
	This work CW Quadrature Radar at 2.4 GHz operating frequency		Seated position	9.31	12.42	Proposed algorithm with single channel signals for 2	
		100				datasets (Subject C at 13b/m and Subject D at 18b/m	
	2.4 G112 operating frequency	4 OHZ Operating frequency				and AD signals for other datasets	
				10.71	14.16	Proposed algorithm with template matching filtering	

even though in some cases single-channel harmonic content is comparable or slightly lower than with AD. This is likely due to single-channel harmonic content sensitivity to phase angle (3) that does not affect AD output.

However, for datasets involving Subject C at 13 b/m and Subject D at 18 b/m, the accuracy of HRV features obtained from the single-channel signal surpasses those obtained with AD. As can be seen from Fig. 5, both second and third harmonic amplitudes are lower in the single-channel signals in these two cases. The performance of circle fitting based on the LM algorithm preceding AD deteriorates when a large phase offset is present. Furthermore, the accuracy of AD is degraded in the presence of a large phase offset inherent in subjects breathing. Consequently, harmonics are not attenuated to a significant extent using AD in these cases, resulting in lower accuracy in beat-to-beat analysis. These cases with high phase offset between the thorax and abdomen motion can be identified through respiration harmonic analysis (Fig. 5) and IQ plots (Fig. 6), and subsequently analyzed using a single channel with a lower harmonic content.

The results given in Table II show agreement between the HRV features (SDNN and RMSSD) acquired from radar and PPG signal. For all the measurements, the average difference of SDNNs between radar and PPG signals varied less than ± 11 ms, while the RMSSDs between the two signals differed less than ± 15 ms. The difference is reduced to ± 9.31 ms for SDNN and ± 12.42 ms for RMSSD when single-channel signal for datasets Subject C at 13 b/m and Subject D at 18 b/m and

AD signal for the rest of the datasets is used. Next, the MAE is used to assess the accuracy of the proposed method and is compared with the state-of-the-art algorithms as shown in Table III [29].

Table III shows a comparison of the proposed method with other published 2.4- and 24-GHz HRV data, that were all captured at a higher sampling rate. Petrovic et al. [7] uses a two-step process Chirp Z transform (CZT) to determine coarse heartbeat followed by a selection of bandpass filter bank and zero-cross peak detection to determine heartbeat peak positions. Here, accuracy was improved using the cascade of FIR bandpass filter bank that increased the computational complexity as well. In [28], a hidden semi-Markov model (HSMM), frequency envelogram, and data segmentation to detect the heart sounds P1 (closure of the mitral valve) and P2 (closure of the pulmonary valve) of cardiac cycles. Although the work reports a higher accuracy in the HRV features, their proposed methods require a spectrogram of high resolution which in turn necessitates a high sampling rate of 50 kHz for data acquisition.

This study demonstrated the best HRV accuracy with 2.4 GHz radar, obtained with the lowest sampling rate of only 100 Hz. The obtained HRV parameter accuracy is within the sampling resolution limit, and sufficient for detecting meaningful changes in ANS activity [30]. Furthermore, this is the first paper to extensively demonstrate the effect of respiration harmonics on both HR and HRV extraction. Previously published papers, related to harmonics reduction

[11], [12], [14], focused on HR extraction only. However, the performance of the proposed method deteriorates in the presence of a large phase offset as the circle fitting becomes incorrect in these cases. As a solution, other demodulation techniques that can enhance HRV analysis and attenuate harmonic interferences even in the presence of high phase offsets are planned to be studied.

VI. CONCLUSION

This article demonstrates the theoretical and experimental sensitivity of respiration harmonic content to demodulation and respiration features, such as phase delay between the abdomen and thorax motion during respiratory effort. Arctangent demodulation with imbalance and dc compensation is used to reduce the harmonic content. The highest reduction in harmonics using AD is reported to be 87.14% and 83.03% with respect to I-channel and Q-channel signals, respectively. An algorithm incorporating multiresolution analysis, MODWT with TMF, is proposed to extract the heart signal from AD signals. The proposed method was tested using human subject data obtained using a 2.4-GHz CW quadrature DR with a 100-Hz sampling rate. HRV parameters, SDNN and RMSSD, were estimated with an accuracy of 12.43 ms compared to a PPG reference. These results present the highest HRV accuracy reported to date using 2.4 GHz DR with a minimal sampling rate.

While AD provided significant accuracy improvement for all datasets, it was found theoretically and confirmed experimentally that high phase delay between thorax and abdomen motion limits the effectiveness of AD. Those cases can be identified based on respiration harmonic content and *IQ* plot features and can be more effectively analyzed using the single channel with the lowest harmonic content. This method demonstrated improvement of 10.71 ms in SDNN, and 14.16 ms in RMSSD, and lowered the overall MAE to 12.43 ms.

Time domain measurements related to average HR have been used to study the cross-sectional association between anxiety and reduced HRV. In the future, the aim is to correlate HRV features, such as SDNN and RMSSD, for noninvasive stress assessment.

REFERENCES

- [1] J. C. Lin, "Noninvasive microwave measurement of respiration," Proc. IEEE, vol. 63, no. 10, p. 1530, Oct. 1975, doi: 10.1109/PROC.1975.9992.
- [2] C. I. Franks, B. H. Brown, and D. M. Johnston, "Contactless respiration monitoring of infants," *Med. Biol. Eng.*, vol. 14, no. 3, pp. 306–312, May 1976, doi: 10.1007/BF02478126.
- [3] M. Hernandez-Aguila, J.-L. Olvera-Cervantes, A.-E. Perez-Ramos, and A. Corona-Chavez, "Methodology for the determination of human respiration rate by using Doppler radar and empirical modal decomposition," *Sci. Rep.*, vol. 12, no. 1, p. 8675, May 2022, doi: 10.1038/s41598-022-12726-z.
- [4] J. N. Sameera, A. D. Droitcour, and O. Boric-Lubecke, "Heart rate detection using single-channel Doppler radar system," in *Proc. 44th Annu. Int. Conf. IEEE Eng. Med. Biol. Soc. (EMBC)*, Jul. 2022, pp. 1953–1956, doi: 10.1109/EMBC48229.2022.9871199.
- [5] W. Massagram, V. M. Lubecke, A. Host-Madsen, and O. Boric-Lubecke, "Assessment of heart rate variability and respiratory sinus arrhythmia via Doppler radar," *IEEE Trans. Microw. Theory Techn.*, vol. 57, no. 10, pp. 2542–2549, Oct. 2009, doi: 10.1109/TMTT.2009.2029716.

- [6] S. Ahmed, Y. Lee, Y.-H. Lim, S.-H. Cho, H.-K. Park, and S. H. Cho, "Noncontact assessment for fatigue based on heart rate variability using IR-UWB radar," *Sci. Rep.*, vol. 12, no. 1, Aug. 2022, Art. no. 14211, doi: 10.1038/s41598-022-18498-w.
- [7] V. L. Petrović, M. M. Jankovic, A. V. Lupšić, V. R. Mihajlović, and J. S. Popović-Božović, "High-accuracy real-time monitoring of heart rate variability using 24 GHz continuous-wave Doppler radar," *IEEE Access*, vol. 7, pp. 74721–74733, 2019, doi: 10.1109/ACCESS.2019.2921240.
- [8] J.-Y. Kim, J.-H. Park, S.-Y. Jang, and J.-R. Yang, "Peak detection algorithm for vital sign detection using Doppler radar sensors," Sensors, vol. 19, no. 7, p. 1575, Apr. 2019, doi: 10.3390/s19071575.
- [9] J. N. Sameera, M. S. Ishrak, V. Lubecke, and O. Boric-Lubecke, "Effect of respiration harmonics on beat-to-beat analysis of heart signal," in *IEEE MTT-S Int. Microw. Symp. Dig.*, Jun. 2023, pp. 1081–1084, doi: 10.1109/IMS37964.2023.10188004.
- [10] C. Li and J. Lin, "Optimal carrier frequency of non-contact vital sign detectors," in *Proc. IEEE Radio Wireless Symp.*, Jan. 2007, pp. 281–284, doi: 10.1109/RWS.2007.351823.
- [11] T.-Y. Huang, L. Hayward, and J. Lin, "Adaptive harmonics comb notch digital filter for measuring heart rate of laboratory rat using a 60-GHz radar," in *IEEE MTT-S Int. Microw. Symp. Dig.*, May 2016, pp. 1–4, doi: 10.1109/MWSYM.2016.7540004.
- [12] J. Tu and J. Lin, "Respiration harmonics cancellation for accurate heart rate measurement in non-contact vital sign detection," in *IEEE MTT-S Int. Microw. Symp. Dig.*, Jun. 2013, pp. 1–3, doi: 10.1109/MWSYM.2013.6697732.
- [13] Y. Ding, X. Yu, C. Lei, Y. Sun, X. Xu, and J. Zhang, "A novel real-time human heart rate estimation method for noncontact vital sign radar detection," *IEEE Access*, vol. 8, pp. 88689–88699, 2020, doi: 10.1109/ACCESS.2020.2993503.
- [14] H. Zhang et al., "The separation of the heartbeat and respiratory signal of a Doppler radar based on the LMS adaptive harmonic cancellation algorithm," in *Proc. 6th Int. Symp. Comput. Intell. Design*, Oct. 2013, pp. 362–364, doi: 10.1109/ISCID.2013.97.
- [15] H. Pan, Y. Zou, and M. Gu, "A spectrum estimation approach for accurate heartbeat detection using Doppler radar based on combination of FTPR and TWV," *EURASIP J. Adv. Signal Process.*, vol. 2022, no. 1, p. 67, Jul. 2022, doi: 10.1186/s13634-022-00899-8.
- [16] O. Boric-Lubecke, V. M. Lubecke, A. D. Droitcour, B.-K. Park, and A. Singh, *Doppler Radar Physiological Sensing*. Hoboken, NJ, USA: Wiley, 2015.
- [17] C. Song, "System-on-chip based Doppler radar occupancy sensor with add-on passive node," Ph.D. dissertation, Dept. Elect. Eng., Univ. Hawaii Manoa, Honolulu, HI, USA, 2014.
- [18] E. Yavari and O. Boric-Lubecke, "Channel imbalance effects and compensation for Doppler radar physiological measurements," *IEEE Trans. Microw. Theory Techn.*, vol. 63, no. 11, pp. 3834–3842, Nov. 2015, doi: 10.1109/TMTT.2015.2484347.
- [19] J. E. Kiriazi, O. Boric-Lubecke, and V. M. Lubecke, "Modeling of human torso time-space characteristics for respiratory effective RCS measurements with Doppler radar," in *IEEE MTT-S Int. Microw. Symp. Dig.*, Jun. 2011, pp. 1–4, doi: 10.1109/MWSYM.2011.5972881.
- [20] X. Gao, A. Singh, E. Yavari, V. Lubecke, and O. Boric-Lubecke, "Non-contact displacement estimation using Doppler radar," in *Proc. Annu. Int. Conf. IEEE Eng. Med. Biol. Soc.*, Aug. 2012, pp. 1602–1605, doi: 10.1109/EMBC.2012.6346251.
- [21] M. Zakrzewski et al., "Quadrature imbalance compensation with ellipse-fitting methods for microwave radar physiological sensing," *IEEE Trans. Microw. Theory Techn.*, vol. 62, no. 6, pp. 1400–1408, Jun. 2014, doi: 10.1109/TMTT.2014.2321738.
- [22] V. Alarcon-Aquino and J. A. Barria, "Change detection in time series using the maximal overlap discrete wavelet transform," *Latin Amer. Appl. Res.*, vol. 39, no. 2, pp. 145–152, Jun. 2009. Accessed: Jul. 9, 2023. [Online]. Available: http://www.scielo.org.ar/scielo.php?pid=S0327-07932009000200009&script=sci_arttext
- [23] Y. Iwata, H. T. Thanh, G. Sun, and K. Ishibashi, "High accuracy heartbeat detection from CW-Doppler radar using singular value decomposition and matched filter," *Sensors*, vol. 21, no. 11, p. 3588, May 2021, doi: 10.3390/s21113588.
- [24] S. Izumi, T. Okano, D. Matsunaga, H. Kawaguchi, and M. Yoshimoto, "Non-contact instantaneous heart rate extraction system using 24-GHz microwave Doppler sensor," *IEICE Trans. Commun.*, vol. E102.B, no. 6, pp. 1088–1096, Jun. 2019.

- [25] R. T. Wakai and W. J. Lutter, "Matched-filter template generation via spatial filtering: Application to fetal biomagnetic recordings," *IEEE Trans. Biomed. Eng.*, vol. 49, no. 10, pp. 1214–1217, Oct. 2002, doi: 10.1109/TBME.2002.803523.
- [26] T. Ursell. 1D Non-Derivative Peak Finder. Accessed: Jul. 7, 2023. [Online]. Available: https://www.mathworks.com/matlabcentral/fileexchange/30490-1d-non-derivative-peak-finder
- [27] F. Shaffer and J. P. Ginsberg, "An overview of heart rate variability metrics and norms," *Frontiers Public Health*, vol. 5, Sep. 2017, Art. no. 258, doi: 10.3389/fpubh.2017.00258.
- [28] W. Xia, Y. Li, and S. Dong, "Radar-based high-accuracy cardiac activity sensing," *IEEE Trans. Instrum. Meas.*, vol. 70, pp. 1–13, 2021, doi: 10.1109/TIM.2021.3050827.
- [29] H. Xu, M. P. Ebrahim, K. Hasan, F. Heydari, P. Howley, and M. R. Yuce, "Accurate heart rate and respiration rate detection based on a higherorder harmonics peak selection method using radar non-contact sensors," *Sensors*, vol. 22, no. 1, p. 83, Dec. 2021, doi: 10.3390/s22010083.
- [30] S. Béres and L. Hejjel, "The minimal sampling frequency of the photoplethysmogram for accurate pulse rate variability parameters in healthy volunteers," *Biomed. Signal Process. Control*, vol. 68, Jul. 2021, Art. no. 102589, doi: 10.1016/j.bspc.2021.102589.



Victor M. Lubecke (Fellow, IEEE) received the B.S. degree in electrical and electronics engineering from the California State Polytechnic University, Pomona, CA, USA, in 1986, and the M.S. and Ph.D. degrees in electrical engineering from the California Institute of Technology, Pasadena, CA, USA, in 1990 and 1995, respectively.

He is currently a Professor of electrical and computer engineering with the University of Hawaii at Manoa, Honolulu, HI, USA. He was previously with Bell Laboratories, Lucent Technologies, Mur-

ray Hill, NJ, USA, where his research focused on remote sensing technologies for biomedical and industrial applications and on microelectromechanical systems (MEMS) and 3-D wafer-scale integration technologies for wireless and optical communications. Before that, he was with the NASA Jet Propulsion Laboratory (JPL), Pasadena, and the Institute for Physical and Chemical Research (RIKEN), Sendai, Japan, where his research involved terahertz and MEMS receiver technologies for space remote sensing and communications applications. He co-founded and served as a CTO for Kai Medical Inc., Honolulu, and co-founded Adnoviv Inc., Honolulu, where he serves as the Vice President. He has authored more than 250 peer-reviewed research articles and holds eight U.S. Patents. His current research interests include remote sensing, biomedical sensors, MEMS, heterogeneous integration, and microwave/terahertz radio.

Prof. Lubecke served as a member for the MTT Technical Committees for Terahertz Technology and Applications and Biological Effects and Medical Applications. He is a Fulbright Scholar, an Emeritus Distinguished Microwave Lecturer of the IEEE Microwave Theory and Techniques (MTT) Society, and a Speakers Bureau Speaker. He has served as a Topic Editor for IEEE TRANSACTIONS ON TERAHERTZ SCIENCE AND TECHNOLOGY and the Vice-Chair for the 2017 IEEE International Microwave Symposium (IMS).



Jannatun Noor Sameera (Graduate Student Member, IEEE) received the B.S. and M.S. degrees in electrical and electronic engineering from the University of Dhaka, Dhaka, Bangladesh, in 2018 and 2020, respectively. She is currently pursuing the Ph.D. degree in electrical and computer engineering with the University of Hawaii at Manoa, Honolulu, HI. USA.

Her current research interests include RF and microwave circuit design and applications, biomedical signal processing, physiological monitoring

sensors, and wireless health monitoring systems.



Olga Boric-Lubecke (Fellow, IEEE) received the B.Sc. degree in electrical engineering from the University of Belgrade, Belgrade, Serbia, in 1989, the M.S. degree in electrical engineering from the California Institute of Technology, Pasadena, CA, USA, in 1990, and the Ph.D. degree in electrical engineering from the University of California at Los Angeles, Los Angeles, CA, USA, in 1995.

She is currently a Professor of electrical and computer engineering with the University of Hawaii at Manoa (UH), Honolulu, HI, USA. Prior to joining

UH, she was with Bell Laboratories, Lucent Technologies, Murray Hill, NJ, USA; the Institute of Physical and Chemical Research (RIKEN), Sendai, Japan; and the NASA Jet Propulsion Laboratory, Pasadena, where she conducted research in RFIC technology and biomedical applications of wireless systems. She co-founded and served as a Chief Technical Advisor for a startup company, Kai Medical, Honolulu, and is also a Co-Founder and the President of Adnoviv Inc., Honolulu. She has authored more than 250 journals and conference publications, two books, and several book chapters. She holds three patents, and her research has been featured by various media outlets. Her current research interests include wireless circuits and systems, biomedical applications, and renewable energy.

Prof. Boric-Lubecke is a Fulbright Scholar, a Foreign Member of the Academy of Engineering of Serbia, and a Distinguished Member of the National Academy of Inventors, UH Chapter. She was a co-recipient of the Emerging Technology Award at TechConnect 2007. She was the adviser–author of several award-winning IEEE Microwave Theory and Techniques Society (IEEE MTT-S) and IEEE Engineering in Medicine and Biology Society (EMB-S) student papers. She has served as the Workshop Chair for the 2003 IEEE IMS, the Technical Program Vice-Chair for the 2007 IEEE IMS, the Technical Program Co-Chair for the 2017 IEEE IMS, and a 2018 IEEE IMS Technical Program Advisor. She has served as an Associate Editor for IEEE MICROWAVE AND WIRELESS COMPONENTS LETTERS and IEEE TRANSACTIONS ON MICROWAVE THEORY AND TECHNIQUES.



Mohammad Shadman Ishrak (Graduate Student Member, IEEE) received the B.Sc. and M.Sc. degrees from the University of Dhaka, Dhaka, Bangladesh, in 2018 and 2020, respectively. He is currently pursuing the Ph.D. degree with the Department of ECE, University of Hawaii at Manoa, Honolulu, HI, USA.

His current work involves the analysis of demodulation techniques and their efficiency of Doppler radar signals for the application. His research interests lie in noninvasive vital sign detection,

cardiorespiratory signal processing, and identity authentication and posture classification through RF sensors.